

# Energy Based Strength Analysis of Fibre Reinforced Polymer Composites

By K.Y. Huang

*Crea Mech Co., Ltd.,*

*Guoshoujing Road 351,*

*201203 Shanghai,*

*People's Republic of China*

*(k.y.huang@crea-mech.com)*

Presented within this paper is a non-linear progressive damage model for predicting the in-plane strength of laminated composites. On the basis of the energy balance principle, the failure criterion is first formulated on the lamina level and subsequently extended to the laminate level, enabling the damage development processes in multidirectional laminates to be analysed in a systematic and structured manner. The key feature of these maximum strain energy based failure criteria is that the failure modes may occur independently under certain circumstances and interactively under other circumstances. The optimized failure prediction algorithm is applicable to symmetrical and balanced laminates that exhibit either fibre dominated or matrix dominated failure behaviour.

**Key words: laminated composites; in-plane strength; failure criteria; progressive damage analysis.**

---

## Nomenclature

|              |                                     |
|--------------|-------------------------------------|
| $A$          | Extensional stiffness matrix        |
| $d$          | Damage parameter                    |
| $\mathbb{D}$ | Damage state matrix                 |
| $E$          | Elastic modulus                     |
| $\mathbb{E}$ | Energy ratio matrix                 |
| $\mathbb{F}$ | Mode interaction matrix             |
| $G$          | Shear modulus                       |
| $N$          | In-plane load                       |
| $Q$          | Reduced stiffness matrix            |
| $S$          | Shear strength or compliance matrix |
| $T$          | Transformation matrix               |
| $V$          | Strain energy per unit volume       |
| $X$          | Longitudinal strength               |
| $Y$          | Transverse strength                 |
| $\gamma$     | Shear strain                        |
| $\epsilon$   | Normal strain                       |
| $\Lambda$    | Interaction parameter               |
| $\nu$        | Poisson's ratio                     |
| $\rho$       | Magnitude of load/strain vector     |
| $\sigma$     | Normal stress                       |
| $\tau$       | Shear stress                        |
| $\Upsilon$   | Failure indicator                   |
| $\Phi$       | Energy ratio                        |
| $\psi$       | Orientation of load/strain vector   |

## 1. Introduction

The in-plane strength of fibre reinforced polymer composites is a subject that has fascinated many scientists and engineers since the introduction of these materials. The beginning of a rational understanding of the strength of isotropic materials is credited to Galileo Galilei (1638), who concluded that failure would occur when the critical stress was attained. The title of his book *Discourses on two new sciences* reflects Galilei's view that the strength of materials is as important as the motion of objects. Over the years, different isotropic failure criteria have been developed by different scientists. In the Coulomb (1776) criterion, failure occurs when the shear stress on the failure plane becomes equal to the sum of the cohesive strength of the material and the friction between the fracture surfaces. The Rankine (1857) criterion uses the maximum normal stresses as the governing physical parameters. The Tresca (1864) criterion is also known as the maximum shear stress criterion that is still employed at present. The Poncelet–Saint-Venant (1870) criterion compares the maximum principal strains with the limiting critical values of the material. In the Beltrami (1885) criterion, yielding occurs when the total strain energy reaches the critical value of the material. In the Mohr (1900) criterion, the failure envelope is calculated by means of Mohr's circle. In the von Mises (Huber 1904, von Mises 1913 and Hencky 1924) criterion that finds favour in present-day structural analyses, yielding of the material is predicted on the basis of the distortion energy.

For unidirectional laminae under combined in-plane stresses, a variety of anisotropic failure criteria have been proposed over the past century (Orifici et al. 2008). The commonly used anisotropic failure criteria can be grouped into the following three classes: non-interactive criteria that comprise the maximum stress and maximum strain criteria; interactive criteria that allow for the full interaction of multi-axial stresses; and hybrid criteria that combine selected aspects of the aforementioned two classes of failure criteria. As is known, the non-interactive criteria generally give non-conservative predictions. The interactive criteria such

as the Norris (1950), Marin (1957), Fischer (1960), Tsai-Hill (1965), Hoffman (1967), Chamis (1969), Tsai-Wu (1971) and Cowin (1979) criteria originate from the Hill (1948) criterion, which is a generalization of the von Mises criterion. The failure criteria in this category tend to be phenomenological and empirical in nature, not mechanistic; they are often criticized for ignoring the diversity of failure modes which are possible (Rowlands 1985 and MIL-HDBK-17 2002). Among the hybrid criteria, the Hashin (1980) criterion that makes use of the stress invariants can be shown to be inconsistent with the classical isotropic failure criteria. In the more complex Puck-Schürmann (1998) and Dávila-Camanho-Rose (2005) criteria, much effort has been expended to modify and to extend the Coulomb-Mohr criterion, which can be viewed as a generalization of the Tresca criterion. In practical terms, the main drawback of the failure criteria along this direction is that a generous number of non-standard material parameters have to be inserted, which can not be readily determined by testing. In brief, none of the existing anisotropic failure criteria is universally satisfactory.

To analyse the failure behaviour of multidirectional laminates, the progressive damage methodology can be applied, which relies on a careful accounting of the sequence of local ply failures leading up to the final laminate failure. During the World-Wide Failure Exercise (WWFE), diverse existing progressive damage models, each incorporating a dissimilar lamina failure criterion, have received a thorough comparison and joint evaluation. At the end of the exercise, the organizers came to the conclusion that the general picture of the damage development in composite materials is still not well understood, as the discrepancies between the theoretical predictions and experimental data remain intolerably large in many cases (Hinton et al. 2004). On the laminate level, the implementation of the lamina failure criteria raises several problems; the most severe of these is apparently the following: it is unclear how the failure modes in the same and different plies interact with each other. If a non-interactive criterion is used on a ply-by-ply basis, the failure envelopes obtained are made up of line

segments connected end to end, where the failure stresses or strains are strongly overestimated in the acute angles. If an interactive criterion is used, the plies after the damage will frequently be stronger than the plies before the damage, ending in various irregular failure envelopes with a zigzag pattern. If a hybrid criterion is used, the interaction between the failure modes will not always occur in the right place and at the right time phrase, as the interactive behaviour is assumed *a priori* and in a certain sense *ad arbitrium*. Hence, the major challenge is to come to a full understanding of the underlying mechanism of the failure mode interaction, so that the progressive damage methodology can be further enhanced to achieve substantially higher accuracy.

Adopting an energetic approach, the complicated failure behaviour of laminated composites under out-of-plane loading can be analytically modelled (Huang et al. 2008 and Huang 2014). It appears that some of the ideas from the energetic school of Ostwald and Mach (Dugas 1955) can be further developed and brought to fruition, thereby enriching the field of mechanics of composite materials. The objective of the present study is to develop a robust and efficient model, which is capable of providing reliable predictions of the failure behaviour of laminated composites under in-plane loading. It is intended to build a new progressive damage model by applying the energy balance principle of Griffith (1920), which states that failure occurs when the energy available in the system is sufficient to overcome the resistance of the material. The energy balance principle can be deduced from the law of conservation of energy, which states that the amount of energy in a closed system remains constant. The model development is guided by the parsimony principle, which states that ‘models should be as simple as possible, but no simpler (Albert Einstein)’. That means that the progressive damage model should be developed in such a way that the simplicity of concept and ease of use is combined with the generality as best as possible. The model validation is undertaken against the experimental data from the WWFE. Finally, conclusions are presented along with future outlooks.

## 2. Lamina Failure Behaviour

To develop a physically well-founded progressive damage model, the best place to start is a unidirectional lamina, which is the basic building block for multidirectional laminates. The interest lies in the theoretical derivation of the failure surfaces of the lamina from the uniaxial stress strain diagrams that can be measured using standardized techniques. The lamina level analysis involves only macromechanical properties and takes full account of the effects of material anisotropy and multiple failure modes. The stresses and strains considered here are planar due to the assumed state of plane stress.

### (a) Constitutive Equations

The uniaxial stress strain diagrams of an orthotropic lamina are shown schematically in figure 1. In the longitudinal direction, the lamina exhibits generally a linear deformation behaviour up to failure, because the deformation is dominated by the fibres. In the transverse and shear directions, the deformation behaviour is non-linear in the large deformation region, as the deformation is dominated by the matrix material. The transverse tensile deformation is virtually linear, because the deformation is limited to a small range. In this study, the transverse compressive deformation is linearized on the basis of the initial stiffness. The highly non-linear shear deformation behaviour can be represented by using the Ramberg-Osgood (1943) equation that consists of a linear and exponential part. If necessary, the transverse compressive deformation can be modelled with the same equation. The endpoints of the stress strain curves are characterized by the longitudinal tensile strength  $X_T$ , the longitudinal compressive strength  $X_C$ , the transverse tensile strength  $Y_T$ , the transverse compressive strength  $Y_C$  and the in-plane shear strength  $S$ . In this paper, all strength values of the material are by definition positive.

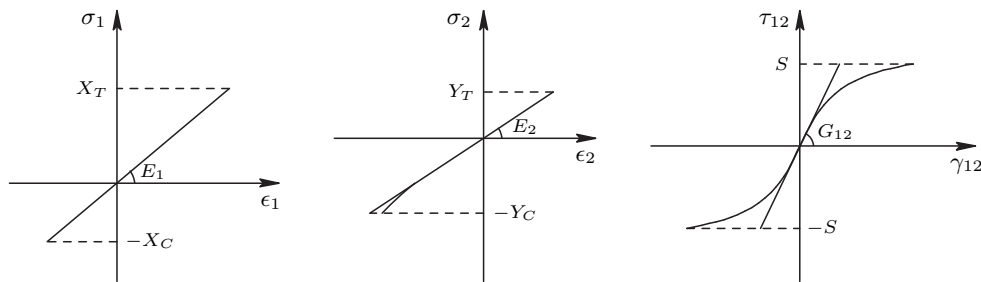


Figure 1. Uniaxial stress strain diagrams of lamina

For the normal deformations, the generalized Hooke's law applies:

$$\begin{Bmatrix} \epsilon_1 \\ \epsilon_2 \end{Bmatrix} = \begin{bmatrix} 1/E_1 & -\nu_{12}/E_1 \\ -\nu_{12}/E_1 & 1/E_2 \end{bmatrix} \begin{Bmatrix} \sigma_1 \\ \sigma_2 \end{Bmatrix} \quad (2.1)$$

where  $\sigma_1$  is the longitudinal stress,  $\sigma_2$  is the transverse stress,  $\epsilon_1$  is the longitudinal strain,  $\epsilon_2$  is the transverse strain,  $E_1$  is the longitudinal elastic modulus,  $E_2$  is the transverse elastic modulus, and  $\nu_{12}$  is the major Poisson's ratio. For the shear deformation, the Ramberg-Osgood equation reads:

$$\gamma_{12} = \frac{\tau_{12}}{G_{12}} + \alpha \left( \frac{\tau_{12}}{S} \right)^\beta \quad (2.2)$$

where  $\tau_{12}$  is the shear stress,  $\gamma_{12}$  is the shear strain,  $G_{12}$  is the shear modulus,  $S$  is the shear strength,  $\alpha$  and  $\beta$  are non-dimensional material constants. Equation (2.2) has an advantage that the integral  $\int \tau_{12} d\gamma_{12}$  can be analytically evaluated, but has a disadvantage that  $\tau_{12}$  has to be numerically calculated from  $\gamma_{12}$ . In Bogetti et al. (2004), an alternative form of the Ramberg-Osgood equation is used, which has an advantage that  $\tau_{12}$  can be readily calculated from  $\gamma_{12}$ , but has a disadvantage that the integral  $\int \tau_{12} d\gamma_{12}$  is analytically unsolvable:

$$\tau_{12} = \frac{G'_{12} \gamma_{12}}{\left[ 1 + \left( \frac{G'_{12} \gamma_{12}}{S'} \right)^\zeta \right]^{1/\zeta}} \quad (2.3)$$

where the initial shear modulus  $G'_{12}$ , the asymptotic stress level  $S'$  and the shape parameter  $\varsigma$  are the constants that fit the empirical data best. For computational considerations, equations (2.2) and (2.3) can be used in parallel, i.e. one for the shear energy evaluation, the other for the strain stress relation. Then it follows that the strain energy stored in the lamina per unit volume is given by:

$$V = \frac{\sigma_1^2}{2E_1} - \frac{\nu_{12}\sigma_1\sigma_2}{E_1} + \frac{\sigma_2^2}{2E_2} + \frac{\tau_{12}^2}{2G_{12}} + \frac{\tau_{12}^{\beta+1}}{K}, \quad K = \frac{\beta+1}{\alpha\beta} S^\beta \quad (2.4)$$

Because of the orthotropic behaviour of the material, there is no coupling between the normal deformations and the shear deformation.

*(b) Deformation and Failure Modes*

As illustrated in figure 2, the deformations in the lamina can be decomposed into the following three modes: the longitudinal deformation mode, the transverse deformation mode and the shear deformation mode. The longitudinal mode occurs due to pure longitudinal tension or compression, the transverse mode occurs due to pure transverse tension or compression, and the shear mode occurs due to pure shear loading. In the transverse mode, the contraction in the longitudinal direction due to the deformation in the transverse direction is neglected, as the longitudinal deformation is dominated by the fibres. For these reasons, the strain energy  $V$  in equation (2.4) is separated into the following three parts:

$$V_I = \frac{\sigma_1^2}{2E_1} - \frac{\nu_{12}\sigma_1\sigma_2}{E_1}, \quad V_{II} = \frac{\sigma_2^2}{2E_2}, \quad V_{III} = \frac{\tau_{12}^2}{2G_{12}} + \frac{\tau_{12}^{\beta+1}}{K} \quad (2.5)$$

where  $V_I$  is the longitudinal deformation energy,  $V_{II}$  is the transverse deformation energy, and  $V_{III}$  is the shear deformation energy.

The failure modes that are expected to occur in the lamina consist of the fibre tensile failure mode, the fibre compressive failure mode, the matrix tensile failure mode, the matrix compressive failure mode and the matrix shear failure mode (see figure 3). For these failure modes, the corresponding strength values are  $X_T$ ,  $X_C$ ,  $Y_T$ ,  $Y_C$  and  $S$ , respectively. On the basis of equations (2.1) and (2.2), the

critical energy of the different failure modes can be expressed as:

$$V_{XT} = \frac{X_T^2}{2E_1}, \quad V_{XC} = \frac{X_C^2}{2E_1}, \quad V_{YT} = \frac{Y_T^2}{2E_2}, \quad V_{YC} = \frac{Y_C^2}{2E_2}, \quad V_S = \frac{S^2}{2G_{12}} + \frac{S^{\beta+1}}{K} \quad (2.6)$$

In line with the deformation modes, the five failure modes are reduced to three failure modes, viz. the longitudinal failure mode, the transverse failure mode and the shear failure mode:

$$V_X = \frac{X^2}{2E_1}, \quad V_Y = \frac{Y^2}{2E_2}, \quad V_S = \frac{S^2}{2G_{12}} + \frac{S^{\beta+1}}{K} \quad (2.7)$$

$$X = H(\sigma_1)X_T + [1 - H(\sigma_1)]X_C \quad (2.8)$$

$$Y = H(\sigma_2)Y_T + [1 - H(\sigma_2)]Y_C$$

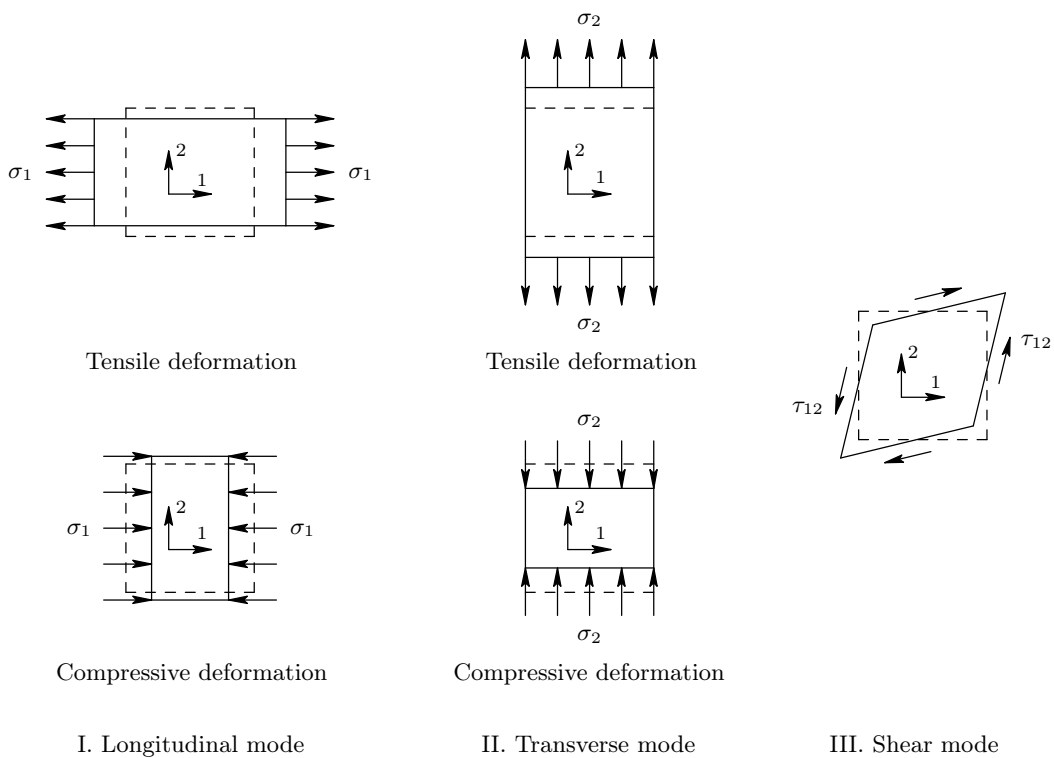


Figure 2. Deformation modes of unidirectional lamina

where  $H$  is the Heaviside step function. This means that  $X = X_T$  for  $\sigma_1 > 0$ ,  $X = X_C$  for  $\sigma_1 < 0$ ,  $X = (X_T + X_C)/2$  for  $\sigma_1 = 0$ ,  $Y = Y_T$  for  $\sigma_2 > 0$ ,  $Y = Y_C$  for  $\sigma_2 < 0$  and  $Y = (Y_T + Y_C)/2$  for  $\sigma_2 = 0$ .

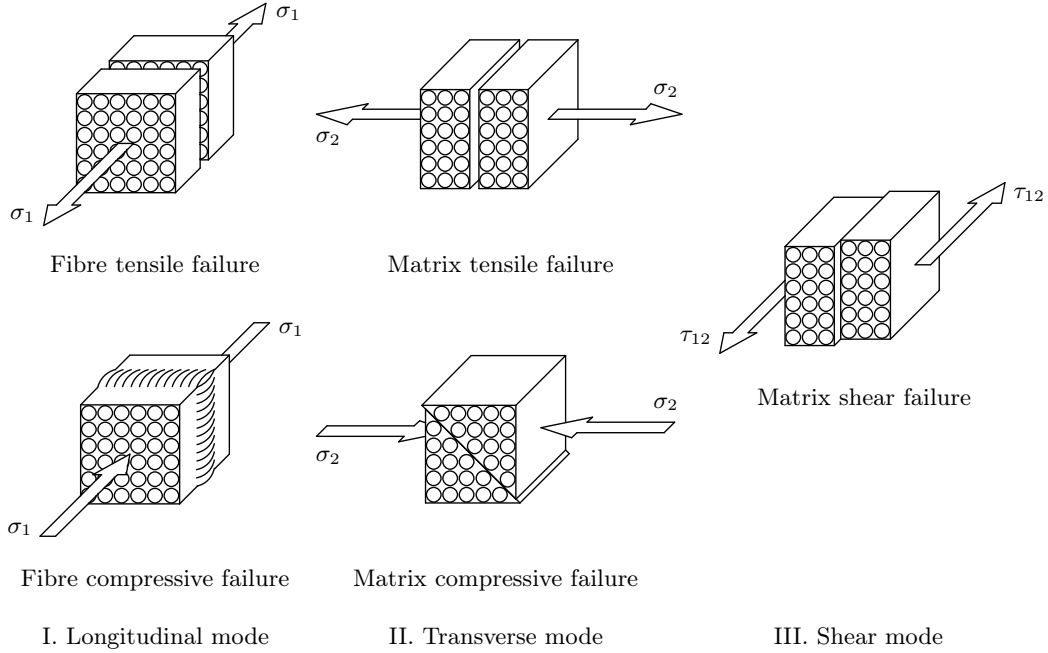


Figure 3. Failure modes of unidirectional lamina

*(c) Lamina Failure Criterion*

As postulated by Griffith (1920), if a crack is in equilibrium, the decrease of strain energy must be equal to the increase of surface energy due to crack extension. For a system with multiple cracks, it seems often more convenient to look at the energy balance in a different perspective, namely from the representative volume instead of the crack area. In point of fact, the energy balance principle can be formulated in a more general form, regardless of whether the material exhibits a brittle or tough behaviour in a certain direction: failure occurs when the energy released from the system equals or exceeds the energy dissipated due to the damage formation. For a unidirectional lamina, it follows

from the energy balance principle that:

$$\begin{aligned}
 & \text{Longitudinal failure occurs, if } V_{\text{I}} \geq V_X; \\
 & \text{Transverse failure occurs, if } V_{\text{II}} \geq V_Y; \\
 & \text{Shear failure occurs, if } V_{\text{III}} \geq V_S.
 \end{aligned} \tag{2.9}$$

As a matter of fact, fracture mechanics and damage mechanics can be thought of as two physically equivalent formulations that have different virtues. This resembles the concept of discrete and continuous systems in the field of dynamics (Meirovitch 1986). As fracture mechanics focuses on the behaviour of the individual cracks, it is suitable to the problems involving one dominant crack or a few large cracks (Anderson 1991). As damage mechanics does not treat the individual cracks, but instead considers the damage state parameters as the key variables, it is advantageous for the problems in which the microcracks are distributed in a statistically homogeneous manner (Allix & Hild 2002). Accordingly, fracture and damage mechanics in a merged form can serve as the foundation of the progressive damage methodology. This resolves the issues such as the conventional fracture mechanics approach is inappropriate for the damage initiation problems and the continuum damage mechanics approach usually demands a laborious micromechanical failure analysis.

On the basis of relations (2.9), the following energy ratios are introduced:

$$\Phi_1 = \frac{V_{\text{I}}}{V_X} = \frac{\sigma_1^2}{X^2} - 2\nu_{12} \frac{\sigma_1 \sigma_2}{X^2}, \quad \Phi_2 = \frac{V_{\text{II}}}{V_Y} = \frac{\sigma_2^2}{Y^2}, \quad \Phi_3 = \frac{V_{\text{III}}}{V_S} = \frac{\frac{\tau_{12}^2}{2G_{12}} + \frac{\tau_{12}^{\beta+1}}{K}}{\frac{S^2}{2G_{12}} + \frac{S^{\beta+1}}{K}} \tag{2.10}$$

The energy ratios can be used to assess whether failure occurs in the material and if so to identify which failure mode occurs. If a non-critical failure mode occurs that does not threaten the structural integrity, it seems plausible to assume that the strain energy stored in the remaining modes remains unchanged, as the structure is still capable of withstanding the applied loads. Therefore, the non-critical modes can be considered to be independent of each other. Setting now the non-critical modes aside, if a critical failure mode occurs that is associated

with the catastrophic failure of the structure, it can be expected that the strain energy in one mode can take occasion to flow to another mode during the unstable damage growth. For this reason, the critical modes are interactive with each other because of the emergence of the energy flow within the system. For a unidirectional lamina, three distinct scenarios have to be analysed as follows. In the first case, all three failure modes are supposed to be critical; failure occurs, when the following expression returns true:

$$\text{NOT}(\Phi_1 \leq 1 \text{ AND } \Phi_2 \leq 1 \text{ AND } \Phi_3 \leq 1) \quad (2.11)$$

In the second case, the failure modes are partly critical; there are three different possibilities:

$$\begin{aligned} &\text{NOT}(\Phi_1 \leq 1 \text{ AND } \Phi_2 \leq 1) \text{ OR } \Phi_3 \geq 1 \\ &\text{NOT}(\Phi_1 \leq 1 \text{ AND } \Phi_3 \leq 1) \text{ OR } \Phi_2 \geq 1 \\ &\text{NOT}(\Phi_2 \leq 1 \text{ AND } \Phi_3 \leq 1) \text{ OR } \Phi_1 \geq 1 \end{aligned} \quad (2.12)$$

In the third case, all three failure modes are non-critical; failure occurs, if the following is satisfied:

$$\Phi_1 \geq 1 \text{ OR } \Phi_2 \geq 1 \text{ OR } \Phi_3 \geq 1 \quad (2.13)$$

In expressions (2.11-2.13), AND, OR and NOT are Boolean operators. For a unidirectional fibre composite, it is known that all three failure modes are critical and therefore interact with each other under practical test conditions. For a lamina embedded within a laminate, the failure mode interaction is a phenomenon that depends upon the laminate configuration and loading conditions; therefore, the criticality of the failure modes has to be determined case-by-case during the progressive damage analysis.

To reduce expressions (2.11-2.13) to one single expression, the following indicator  $\Lambda$  is introduced:

$$\Lambda_j = \begin{cases} 1 & \text{if failure mode is critical} \\ 0 & \text{if failure mode is non-critical} \end{cases} \quad (2.14)$$

where  $j = 1, 2, 3$ . For the critical modes, the domain enclosed by the failure surface is given by:

$$(\Lambda_1\Phi_1 - 1)(\Lambda_2\Phi_2 - 1)(\Lambda_3\Phi_3 - 1) \leq 0 \quad (2.15)$$

Expanding relation (2.15) and discarding the higher order terms, the following relation can be obtained:

$$\Upsilon = \Lambda_1\Phi_1 + \Lambda_2\Phi_2 + \Lambda_3\Phi_3 \leq 1 \quad (2.16)$$

For the non-critical modes, there holds:

$$\Upsilon' = \max(\Lambda'_1\Phi_1, \Lambda'_2\Phi_2, \Lambda'_3\Phi_3) \leq 1, \quad \Lambda'_j = 1 - \Lambda_j \quad (2.17)$$

Combining relations (2.16) and (2.17) with each other, the general failure criterion for the unidirectional lamina becomes then:

$$\max(\Upsilon, \Upsilon') = 1 \quad (2.18)$$

In the three-dimensional energy space  $V_I$ - $V_{II}$ - $V_{III}$ , the failure surfaces of the lamina can be geometrically interpreted as the front surfaces of a tetrahedron, a prism or a cuboid (see figure 4).

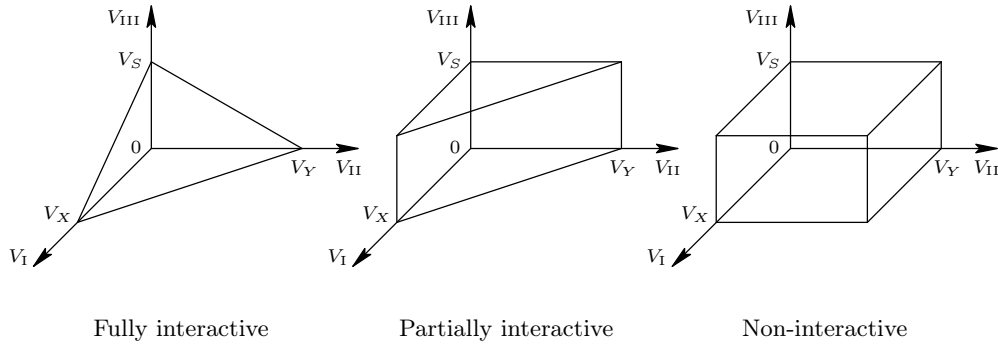


Figure 4. Different failure surfaces of unidirectional lamina

(d) *Alternative formulation*

Instead of the principal stresses  $\sigma_1$ ,  $\sigma_2$  and  $\tau_{12}$ , it is also possible to define the deformation and failure modes on the basis of the principal strains  $\epsilon_1$ ,  $\epsilon_2$  and  $\gamma_{12}$ . In this way, a second variant of the lamina failure criterion can be obtained:

$$\max(\widehat{\Upsilon}, \widehat{\Upsilon}') = 1 \quad (2.19)$$

with

$$\widehat{\Phi}_1 = \frac{\epsilon_1^2}{\epsilon_1^{u2}} + \frac{2\nu_{21}\epsilon_1\epsilon_2}{\epsilon_1^{u2}} \approx \frac{\epsilon_1^2}{\epsilon_1^{u2}}, \quad \widehat{\Phi}_2 = \frac{\epsilon_2^2}{\epsilon_2^{u2}}, \quad \widehat{\Phi}_3 = \frac{\int_0^{\gamma_{12}} \tau_{12} d\gamma_{12}}{\int_0^{\gamma_{12}^u} \tau_{12} d\gamma_{12}} \quad (2.20)$$

where  $\widehat{\Upsilon}$  and  $\widehat{\Upsilon}'$  are calculated in the same manner as  $\Upsilon$  and  $\Upsilon'$ . For clarity, it should be mentioned that the second set of energy ratios  $\widehat{\Phi}_j$  is derived using the simplification  $1 - \nu_{12}\nu_{21} \approx 1$ . In  $\widehat{\Phi}_1$ ,  $\widehat{\Phi}_2$  and  $\widehat{\Phi}_3$ ,  $\gamma_{12}^u$  is the shear failure strain, and the failure strains  $\epsilon_1^u$  and  $\epsilon_2^u$  are given by:

$$\begin{aligned} \epsilon_1^u &= H(\epsilon_1)\epsilon_{1T} + [1 - H(\epsilon_1)]\epsilon_{1C} \\ \epsilon_2^u &= H(\epsilon_2)\epsilon_{2T} + [1 - H(\epsilon_2)]\epsilon_{2C} \end{aligned} \quad (2.21)$$

For a self-consistent dataset,  $\epsilon_{1T}$ ,  $\epsilon_{1C}$ ,  $\epsilon_{2T}$ ,  $\epsilon_{2C}$  and  $\gamma_{12}^u$  can be calculated from  $X_T$ ,  $X_C$ ,  $Y_T$ ,  $Y_C$  and  $S$  by using the Hooke's law and the Ramberg-Osgood equation.

In the remainder of this paper, the two variants that are similar in most respects are called the stress and strain variant of the lamina failure criterion, respectively. It is noteworthy that the transverse failure, which is exclusively controlled by the transverse deformation in the strain variant, is also affected by the longitudinal deformation in the stress variant. This means that the influence of the fibres in the stress variant is somewhat stronger than in the strain variant. On the lamina level, the choice of the stress or strain variant depends on whether the testing condition is load or displacement controlled. On the laminate level, the stress variant is better suited for fibre dominated laminates, whilst the strain variant is better suited for matrix dominated laminates.

(e) *Comparison with Existing Failure Criteria*

For the non-interactive case  $\Lambda_1 = \Lambda_2 = \Lambda_3 = 0$ , equation (2.18) can be simplified to the maximum stress criterion:

$$\max \left( \left| \frac{\sigma_1}{X} \right|, \left| \frac{\sigma_2}{Y} \right|, \left| \frac{\tau_{12}}{S} \right| \right) = 1 \quad (2.22)$$

and equation (2.19) can be simplified to the maximum strain criterion:

$$\max \left( \left| \frac{\epsilon_1}{\epsilon_1^u} \right|, \left| \frac{\epsilon_2}{\epsilon_2^u} \right|, \left| \frac{\gamma_{12}}{\gamma_{12}^u} \right| \right) = 1 \quad (2.23)$$

Linearizing the shear deformation, equation (2.18) can be reduced to the following quadratic form for the fully interactive case  $\Lambda_1 = \Lambda_2 = \Lambda_3 = 1$ :

$$\frac{\sigma_1^2}{X^2} - 2\nu_{12} \frac{\sigma_1 \sigma_2}{X^2} + \frac{\sigma_2^2}{Y^2} + \frac{\tau_{12}^2}{S^2} = 1 \quad (2.24)$$

It can be seen that equation (2.24) is a generalization of the maximum strain energy based yield criterion of isotropic materials, which was originally pioneered by Beltrami but did not find widespread application for a long time. Assuming the plastic incompressibility ( $\nu_{12} = 0.5$ , a concept that stems directly from the field of fluid mechanics), equation (2.24) becomes identical to the Hill yield criterion under a plane stress state. It is logical that the current failure criterion reduces to the Beltrami criterion in the limit, which is in a certain sense more versatile than the von Mises criterion. The essential assumption in the von Mises criterion is that materials do not yield under a hydrostatic stress. Therefore, the stresses in a material are separated into a hydrostatic part that causes a volume change and a deviatoric part that causes a shape change of the material. The von Mises criterion is based on the invariant of the deviatoric stress tensor, which can be linked together with the distortion energy. In contrast with isotropic materials, fibre reinforced polymer composite materials are strongly heterogenous and anisotropic in nature. This implies that a hydrostatic stress on the macromechanical level inevitably induces distortions on the micromechanical level, and the material must fail if the stress level is sufficiently high. This justifies why the current failure

criterion in equation (2.18) or (2.19) is formulated on the basis of the strain energy in its totality, without separating the deviatoric and hydrostatic stresses from each other on the macromechanical scale.

The behaviour of a system with a single crack obeys the same laws of physics as a system with multiple cracks. Take the three kinematically admissible crack extension modes introduced by Irwin (1958), viz. the opening, shearing and tearing mode, the energy criterion for crack propagation can be extended on the analogy of the failure criterion (2.18) or (2.19) as follows:

$$\max \left( \sum_{i=I}^{III} \frac{\Lambda_i G_i}{G_{iC}}, \frac{\Lambda'_I G_I}{G_{IC}}, \frac{\Lambda'_II G_{II}}{G_{IIC}}, \frac{\Lambda'_{III} G_{III}}{G_{IIIC}} \right) = 1 \quad (2.25)$$

where  $G_I$ ,  $G_{II}$  and  $G_{III}$  are the strain energy release rates of the three fundamental fracture modes;  $G_{IC}$ ,  $G_{IIC}$  and  $G_{IIIC}$  are the critical energy release rates of the material;  $\Lambda_i$  are the indicators for the mode interaction,  $\Lambda'_i = 1 - \Lambda_i$ . The occurrence of the fracture mode interaction depends on whether the strain energy can flow from one deformation mode to another and *vice versa*. Due to the interaction, the fracture mode with the maximum energy release rate ratio becomes active, while the other modes remain non-active. Under a varying loading condition, it can be argued that the different fracture modes occur frequently in a sequential manner. The terminology mixed-mode is therefore referred to as the deformation modes at the crack tip rather than the fracture modes themselves.

For the fatigue problems, the comparison between the failure criteria leads to the reinterpretation of the cumulative damage rule that was first proposed by Palmgren (1924) and later popularized by Miner (1945). Suppose that there are  $k$  different stress magnitudes in a spectrum, each contributing  $n_i$  cycles, and  $N_i$  is the number of cycles to failure of the  $i$ -th stress amplitude, the Palmgren-Miner rule can be derived in a similar way as the interactive part of the failure criterion (2.18) or (2.19):

$$n_i \leq N_i, \quad i = 1, 2, \dots, k \quad (2.26)$$

$$\left(1 - \frac{n_1}{N_1}\right) \left(1 - \frac{n_2}{N_2}\right) \cdots \left(1 - \frac{n_k}{N_k}\right) \geq 0 \Rightarrow \sum_{i=1}^k \frac{n_i}{N_i} \leq 1 \quad (2.27)$$

As a matter of fact, the  $N_i$  values from the  $SN$ -curve (the Wöhler curve) are measured using initially undamaged specimens; therefore, the gradual deterioration of the material is not properly accounted for in the fatigue process, resulting in a non-conservative prediction. Hence, it is necessary to consider  $N_i$  as a function of at least two variables, namely the stress amplitude  $S_i$  and the damage parameter  $D_i$ . To allow better utilization of the experimental data, the three-dimensional  $N(S, D)$ -surface can be constructed instead of the  $SN$ -curve. As the damage state changes in the course of the fatigue process, the corresponding  $N_i$  values should be substituted into the Palmgren-Miner rule, so that the fatigue life of structures can be evaluated with sufficient engineering accuracy.

### 3. Progressive Damage Analysis

Aimed at a basic strength model, the present study is restricted to unnotched symmetrical balanced laminates under combined in-plane loads. In the aerospace industry, the designers use preferably the fibre dominated laminates; however, the matrix dominated laminates can not be excluded from consideration, since these laminates are still usable and the matrix dominated failure can be precluded due to appropriate choices on a higher structural level during the design phase. In the current model, the failure modes consist solely of the intralaminar modes, viz. the longitudinal, transverse and shear failure mode; the interlaminar mode (the delamination mode) is left out of consideration. The changes of in-plane stiffnesses associated with fibre rotations and the residual stresses in the polymer matrix due to the manufacturing processes are neglected for the sake of convenience. Because of the damage development and the non-linear shear behaviour, the mechanical response of a laminate to a prescribed set of loads or strains has to be calculated through an incremental approach.

(a) *Global Structural Response*

As is customary, the constitutive behaviour of a multidirectional laminate is described using the Classical Lamination Theory (CLT, Jones 1998):

$$\{N\}_n^{i+1} - \{N\}_n^i = [A]_n^i (\{\epsilon\}_n^{i+1} - \{\epsilon\}_n^i) \quad (3.1)$$

where  $\{N\}$  is the vector of the stress resultants,  $\{N\} = \{N_x, N_y, N_{xy}\}^T$ ;  $\{\epsilon\}$  is the vector of the mid-surface strains,  $\{\epsilon\} = \{\epsilon_x, \epsilon_y, \gamma_{xy}\}^T$ . The superscript  $i$  indicates the discrete points, and the subscript  $n$  indicates the failure points. The tangent stiffness matrix  $[A]_n^i$  can be written as:

$$[A]_n^i = \sum_{k=1}^N (t_k [T]_k^{-1} [Q]_{kn}^i [T]_k^{-T}) \quad (3.2)$$

where  $N$  is the total number of the plies and  $t_k$  is the thickness of the  $k$ -th ply. The transformation matrix  $[T]_k$  of the  $k$ -th ply is given by:

$$[T]_k = \begin{bmatrix} \cos^2 \theta_k & \sin^2 \theta_k & 2 \sin \theta_k \cos \theta_k \\ \sin^2 \theta_k & \cos^2 \theta_k & -2 \sin \theta_k \cos \theta_k \\ -\sin \theta_k \cos \theta_k & \sin \theta_k \cos \theta_k & \cos^2 \theta_k - \sin^2 \theta_k \end{bmatrix} \quad (3.3)$$

where  $\theta_k$  is the ply orientation angle. Taking the effects of the damage induced elastic property degradation into account, the components of the reduced stiffness matrix  $[Q]_{kn}^i$  of the  $k$ -th ply become:

$$Q_{11kn}^i = (1 - \eta d_{1kn}) E_1 \quad (3.4)$$

$$Q_{22kn}^i = (1 - \eta d_{2kn}) E_2 \quad (3.5)$$

$$Q_{12kn}^i = (1 - \eta d_{1kn})(1 - \eta d_{2kn}) \nu_{12} E_2 \quad (3.6)$$

$$Q_{66kn}^i = (1 - \eta d_{3kn}) G'_{12} \left[ 1 + \left( \frac{G'_{12} \gamma_{12kn}^i}{S'} \right)^\zeta \right]^{- (1+1/\zeta)} \quad (3.7)$$

$$Q_{16kn}^i = Q_{26kn}^i = 0 \quad (3.8)$$

where the term  $\nu_{12}\nu_{21}$  has been neglected compared to 1, and the damage parameters can be defined as:

$$d_{jkn} = \begin{cases} 0 & \text{before failure} \\ 1 & \text{after failure} \end{cases} \quad (3.9)$$

In this way, a failed ply is assumed to exhibit ideally plastic deformation behaviour on the macromechanical scale. This simplification obviates the need to model the detailed failure processes on the micromechanical scale, and furthermore leads to conservative strength predictions. For the rest, the numerical parameter  $\eta$  has a default value of 0.99. This means that the degraded elastic properties are not exactly 0, but rather effectively 0. Therefore, the stiffness matrix  $[A]_n^i$  is non-singular and always invertible during the analysis.

(b) *Loading Conditions*

Using the spherical coordinates, the in-plane loads with constant mutual ratios can be parameterized by:

$$\{N\}_n^i = \rho_n^i \{\psi\}, \quad \{\psi\} = \{\sin \vartheta \cos \varphi, \sin \vartheta \sin \varphi, \cos \vartheta\}^T \quad (3.10)$$

where  $\vartheta \in [0, \pi]$  and  $\varphi \in [0, 2\pi]$ . For a given orientation vector  $\{\psi\}$ , the magnitude of the load vector can be increased from 0 in equal incremental steps as follows:

$$\rho_n^{i+1} = \rho_n^i + \Delta\rho \quad (3.11)$$

Varying the angles  $\vartheta$  and  $\varphi$  step by step within the specified ranges, the entire three-dimensional failure space can be scanned with an intended resolution. Using equation (3.1), the mid-surface strains at the point  $i+1$  can be calculated with:

$$\{\epsilon\}_n^{i+1} = \{\epsilon\}_n^i + \Delta\rho [S]_n^i \{\psi\} \quad (3.12)$$

where the compliance matrix  $[S]_n^i$  can be obtained by inverting the stiffness matrix  $[A]_n^i$  with Cramer's rule. In case the mid-surface strains are prescribed, equations

(3.10-3.12) can be replaced by:

$$\{\epsilon\}_n^i = \hat{\rho}_n^i \{\psi\}, \quad \hat{\rho}_n^{i+1} = \hat{\rho}_n^i + \Delta\hat{\rho} \quad (3.13)$$

The user parameters  $\Delta\rho$  and  $\Delta\hat{\rho}$  are dependent on the magnitudes of the shear deformations in the plies. If the deformation behaviour of the laminate is as yet unknown, a sensitivity study is helpful in finding the best practical compromise between the predictive accuracy and the computational effort.

(c) *Laminate Failure Criterion and Termination Criteria*

Consider the entire laminate as a system, the lamina failure criterion (2.18) and (2.19) can be extended to a laminate failure criterion by taking the interaction of the failure modes in different plies into account. Starting from an arbitrary failure point  $n$ , the failure point  $n+1$  can be calculated by using:

$$\max(\Upsilon_n, \Upsilon'_n) = 1, \quad \Upsilon_n = \sum_{j=1}^3 \sum_{k=1}^N \frac{\Lambda_{jk} \Phi_{jkn}^p}{\zeta_{jk}}, \quad \Upsilon'_n = \max(\Lambda'_{jk} \Phi_{jkn}^p) \quad (3.14)$$

or

$$\max(\hat{\Upsilon}_n, \hat{\Upsilon}'_n) = 1, \quad \hat{\Upsilon}_n = \sum_{j=1}^3 \sum_{k=1}^N \frac{\Lambda_{jk} \hat{\Phi}_{jkn}^p}{\zeta_{jk}}, \quad \hat{\Upsilon}'_n = \max(\Lambda'_{jk} \hat{\Phi}_{jkn}^p) \quad (3.15)$$

where the superscript  $p$  denotes the last calculated discrete point. Equations (3.14) and (3.15) are called the stress variant and the strain variant of the laminate failure criterion, respectively. Physically the laminate failure criterion means that the critical modes in all plies interact with each other, as a laminate is two or more laminae bonded together to act as an integral structural element. There is no mutual interaction between the non-critical modes, since the strain energy in one mode can not flow into another mode because of the kinematical constraints of the adjacent plies. As a simplification of reality, it is supposed that failure occurs simultaneously in the symmetrical plies and in some anti-symmetrical plies, since the stress components are all the same in the idealized sense. For this reason, these plies can be treated as a single layer during the analysis; therefore, the factor  $\zeta_{jk}$

is equal to the number of the synchronically failing plies. The determination of the interaction parameters  $\Lambda_{jk}$  will be presented in §3d(ii).

If a laminate exhibits a fibre dominated behaviour, the final failure is characterized by the occurrence of the fibre failure:

$$\max(d_{1k\ell}) = 1, \quad k \in [1, \dots, N] \quad (3.16)$$

where the subscript  $\ell$  denotes the last calculated failure point. For a matrix dominated laminate, there are two different situations: in the fibre dominated regions, the final failure can be detected through equation (3.16); in the matrix dominated regions, the final failure can be determined on the basis of the condition of the stiffness matrix  $A_\ell^p$ . When the accumulation of the matrix failures leads to the disintegration of the laminate without breaking the fibres, it is typical that the stiffness matrix becomes badly conditioned so that a small perturbation in the applied loads produces an uncontrolled increase in the mid-surface strains:

$$\varkappa_\ell \gg \varkappa_0 \quad (3.17)$$

where the condition numbers  $\varkappa_\ell$  and  $\varkappa_0$  are based on the spectral norm, i.e.  $\varkappa_\ell = \|[A]_\ell^p\| \cdot \|\text{inv}[A]_\ell^p\|$  and  $\varkappa_0 = \|[A]_0^0\| \cdot \|\text{inv}[A]_0^0\|$ . The threshold value of  $\varkappa_\ell/\varkappa_0$  that is dependent on the parameter  $\eta$  can be determined through numerical experiments. For an angle-ply laminate, use can also be made of the so-called shear failure cutoff, which is a more stringent criterion than relation (3.17):

$$\max(d_{3k\ell}) = 1, \quad k \in [1, \dots, N] \quad (3.18)$$

For the ultimate load carrying capacity of the laminate, the analysis can be terminated, when the final failure point has been reached.

## (d) Failure Prediction Algorithm

From the programming viewpoint, particularly the data storage, it seems convenient to introduce some auxiliary matrices of the same format as follows:

$$[\mathbb{D}]_n = \begin{bmatrix} d_{11n} & \cdots & d_{1kn} & \cdots & d_{1Nn} \\ d_{21n} & \cdots & d_{2kn} & \cdots & d_{2Nn} \\ d_{31n} & \cdots & d_{3kn} & \cdots & d_{3Nn} \end{bmatrix} \quad (3.19)$$

$$[\mathbb{F}] = \begin{bmatrix} \Lambda_{11} & \cdots & \Lambda_{1k} & \cdots & \Lambda_{1N} \\ \Lambda_{21} & \cdots & \Lambda_{2k} & \cdots & \Lambda_{2N} \\ \Lambda_{31} & \cdots & \Lambda_{3k} & \cdots & \Lambda_{3N} \end{bmatrix} \quad (3.20)$$

$$[\mathbb{E}]_n = \begin{bmatrix} \Phi_{11n}^p & \cdots & \Phi_{1kn}^p & \cdots & \Phi_{1Nn}^p \\ \Phi_{21n}^p & \cdots & \Phi_{2kn}^p & \cdots & \Phi_{2Nn}^p \\ \Phi_{31n}^p & \cdots & \Phi_{3kn}^p & \cdots & \Phi_{3Nn}^p \end{bmatrix} \quad (3.21)$$

$$[\widehat{\mathbb{E}}]_n = \begin{bmatrix} \widehat{\Phi}_{11n}^p & \cdots & \widehat{\Phi}_{1kn}^p & \cdots & \widehat{\Phi}_{1Nn}^p \\ \widehat{\Phi}_{21n}^p & \cdots & \widehat{\Phi}_{2kn}^p & \cdots & \widehat{\Phi}_{2Nn}^p \\ \widehat{\Phi}_{31n}^p & \cdots & \widehat{\Phi}_{3kn}^p & \cdots & \widehat{\Phi}_{3Nn}^p \end{bmatrix} \quad (3.22)$$

where  $[\mathbb{D}]_n$  is the damage state matrix and  $[\mathbb{F}]$  is the mode interaction matrix that is  $n$  independent. Among the twinned energy ratio matrices,  $[\mathbb{E}]_n$  is based on the stress variant (3.14) and  $[\widehat{\mathbb{E}}]_n$  is based on the strain variant (3.15). In  $[\mathbb{E}]_n$  and  $[\widehat{\mathbb{E}}]_n$ , the values of the point  $i$  are overwritten by the values of the point  $i+1$ .

In broad outlines, the current progressive damage analysis is based on a predictor-corrector scheme:

**Step 1.** The failure surface of the first order is simulated by fully neglecting the failure mode interaction. Suppose that the failure point  $n$  is known, the load level is further increased to such an extent that the stress variant of the laminate failure criterion (3.14) has just been satisfied:

$$\max([\mathbb{E}]_n) \geq 1 \quad (3.23)$$

The variable  $\rho_{n+1}^p$  can be solved by using the bisection method, where the last two calculated points form the lower and upper bound. Compared with the Newton-Raphson method, the bisection method uses only function values (no derivative values) and is especially suitable for noisy functions, although its convergence rate is relatively low. Locating the maximum components in the energy ratio matrix  $[\mathbb{E}]_n$ , it can be determined which failure mode has occurred and which plies have failed at the failure point  $n+1$ . For the failure point  $n+2$ , the damage state matrix  $[\mathbb{D}]_n$  is updated to  $[\mathbb{D}]_{n+1}$ . The calculations are repeated until one of the termination criteria (3.16), (3.17) or (3.18) is satisfied. When the entire failure surface is prescanned, the predictor step is finished, and one proceeds to the next step.

**Step 2.** The failure surface obtained is upgraded to the second order by taking the failure mode interaction into account. In doing so, a survey is made of the critical failure modes for all possible loading conditions. In the  $[\mathbb{F}]$  matrix, the mode interaction parameters  $\Lambda_{jk}$  that correspond to the critical modes become 1, while the other components correspond to the non-critical modes remain 0. If the  $[\mathbb{F}]$  matrix shows that the laminate is fibre dominated, the interactive failure surface is calculated in an incremental way by proceeding with the last non-critical points from the predictor step:

$$\sum_{j=1}^3 \sum_{k=1}^N \frac{\Lambda_{jk} \Phi_{jkn}^p}{\zeta_{jk}} = 1 \quad (3.24)$$

For equation (3.24), the aforementioned bisection solver remains available. If the laminate is matrix dominated, the interactive failure surface can be calculated from the beginning on the basis of the strain variant of the laminate failure criterion (3.15). After the final scan has been performed systematically on the failure surface, the corrector step as well as the whole progressive damage analysis are finished.

Regarding the model implementation and virtual material testing, the commercial mathematics software package Matlab<sup>TM</sup> can be employed, which integrates programming, computation and visualization in a user-friendly environment. So far, the development of the progressive damage model for in-plane failures of multidirectional laminates has been completed, where the energy based failure criterion with allowance for proper failure mode interactions and the precise failure mode scanning technique make this model unique among many other models that can be found in the open literature.

#### 4. Experimental Verification

The accuracy of the progressive damage model is verified on the basis of the WWFE benchmark data, which were obtained by subjecting thin-walled tubes to combinations of internal or external pressure, axial load and torsion. Seven test cases are analysed, which cover the following three types of laminates:

- E-glass/MY750  $[\pm 55^\circ]_S$  laminate
- E-glass/LY556  $[90^\circ/\pm 30^\circ]_S$  laminate
- AS4/3501-6  $[0^\circ/\pm 45^\circ/90^\circ]_S$  laminate

The theoretical and experimental results that comprise a number of stress strain diagrams and biaxial failure envelopes are compared with each other in a critical manner, where the emphasis is placed on the physical interpretations of the results rather than the mathematical correlations between the results. For the mechanical properties of the unidirectional laminae, the reader is referred to Hinton et al. (2004).

##### (a) *E-glass/MY750 Angle-ply Laminate*

In figure 5, it can be seen that the theoretical structural response is in good agreement with the experimental data points. The stress strain curves are highly

non-linear, as the plies undergo significant shear deformations due to the uniaxial loading. When the transverse and shear stiffnesses of the plies are reduced to almost 0 ( $\eta \approx 1$ ), the laminate becomes unstable at the shear failure point, where the stiffness matrix becomes badly conditioned. In this way, an idealized lower bound is found for the final failure. If the elastic property degradation is discarded ( $\eta = 0$ ), the three failure points that occur in succession are of the transverse, shear and longitudinal failure mode, respectively. This upper bound of the final failure occurs, when the plies with matrix cracks coincidentally have some residual stiffness so that the laminate remains capable of carrying additional loads until the level of fibre failure is reached. From a practical standpoint, the calculations which follow are performed with  $\eta \approx 1$ .

On the strain plane the biaxial failure envelope of the laminate is constructed by means of the maximum strain criterion, as shown in figure 6. From the failure strain contour, it can be verified that fibre rotation occurs only to a minor extent. The equation that relates the realigned angle  $\theta'$  of a ply to the original angle  $\theta$  reads  $\theta' = \arctan[\tan \theta(1 + \epsilon_y)/(1 + \epsilon_x)]$  (see Hinton et al. (2004)). When an angle-ply laminate is subjected to large deformations, the linearization of the transverse deformation behaviour of the plies leads to an over-estimation of the

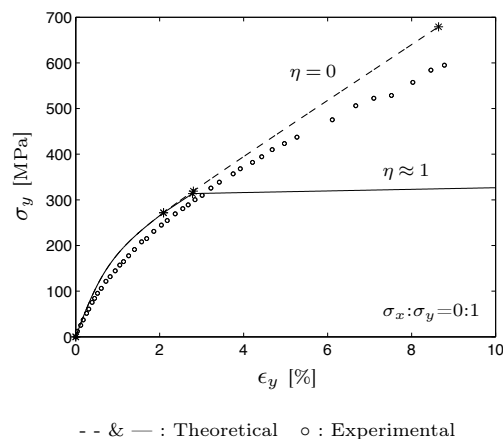


Figure 5. Stress strain diagrams of  $[\pm 55^\circ]_s$  laminate

laminates in-plane stiffnesses. To obtain a conservative last-ply failure prediction, the transverse modulus  $E_2$  of the plies is reduced to 0 as is done in the netting analysis (see MIL-HDBK-17 2002). The shear modulus  $G_{12}$  is retained, as the shear deformations are in the ascendant. The first-ply failures are evaluated through a separate analysis with input of the unmodified transverse ply stiffness, as it can be supposed that the ply deformations are relatively small. From the failure envelope on the stress plane, it can be seen that the theoretical calculations are consistent with the bulk of the experimental data (see figure 6). In view of the basic equations used, it is logical that the current model provides the same first-ply failure results as the non-linear model of Bogetti et al. (2004), and nearly the same first order last-ply failure results as the graphical method of Hart-Smith (1998). The maximum strength of the laminate occurs in the direction  $\sigma_x:\sigma_y=1:2$ , where the applied loads are efficiently transferred into the fibres. The remaining regions are dominated by the matrix shear failures. The second order failure envelope shows further that the interaction between the longitudinal and shear failure modes occurs primarily in the acute angles. The experimental data points outside

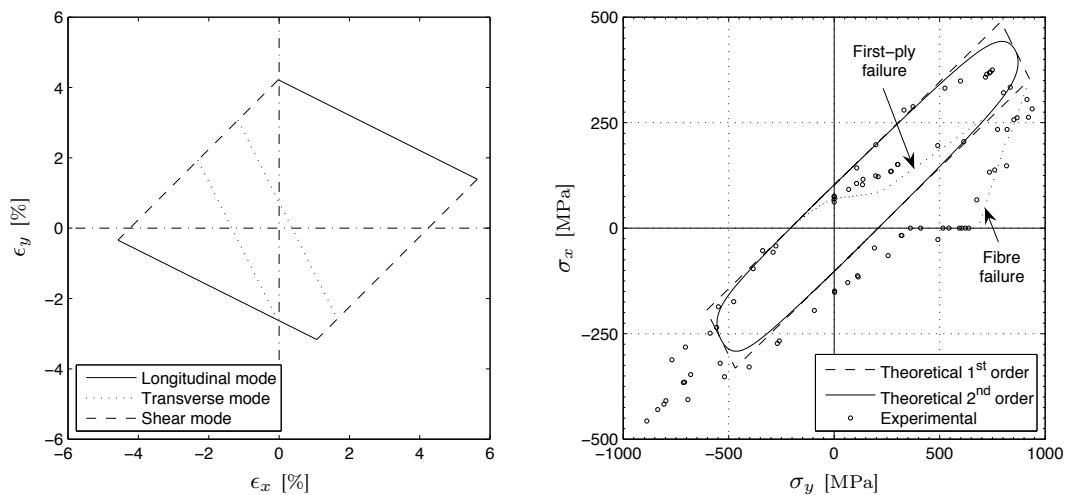


Figure 6. Failure envelopes of  $[\pm 55^\circ]_S$  laminate on strain and stress plane

the elongated failure envelope can be simulated by giving the damaged plies a certain residual transverse and shear stiffness (e.g.  $\eta = 0.5$ ).

(b) *E-glass/LY556 Multidirectional Laminate*

Due to the large stiffness mismatch, the  $[90^\circ/\pm 30^\circ]_S$  laminate is vulnerable to delaminations along the  $90^\circ/30^\circ$  and  $30^\circ/90^\circ$  interfaces. For the final failure envelopes, the laminate is thought of as the delaminated  $[\pm 30^\circ]_S$  sublaminate sandwiched between two thinner  $[90^\circ]$  sublaminates, where the strains in the different plies remain equal to each other. Based on the experience in the previous  $[\pm 55^\circ]_S$  laminate, the transverse modulus  $E_2$  of the  $\pm 30^\circ$  plies is reduced to 0. It turns out that the theoretical predictions agree reasonably well with the experimental data (see figure 7). The first order  $\sigma_x$ - $\sigma_y$  graph shows that the ultimate strength of the laminate is controlled by the longitudinal failure modes in the  $90^\circ$  plies and the  $\pm 30^\circ$  plies that fail contemporaneously. The strong asymmetry in the second order failure envelope is attributed to the large differences in the stiffness and strength properties of the  $[90^\circ]$  sublaminates and the  $[\pm 30^\circ]_S$  sublaminate. In the compression-compression quadrant, it is likely

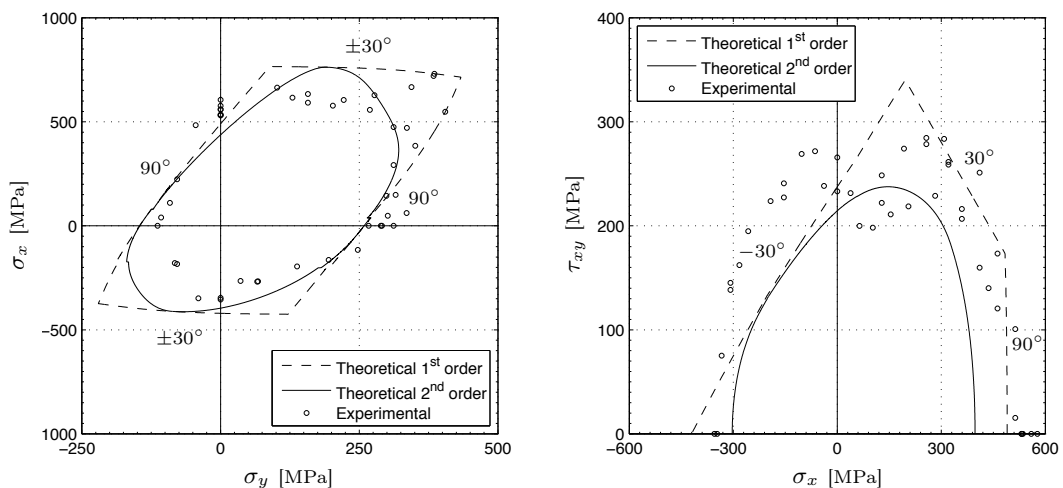


Figure 7. Failure envelopes of  $[90^\circ / \pm 30^\circ]_S$  laminate

that a premature failure mechanism such as buckling has occurred during the tests, i.e. these data points can be identified as outliers. Under the combined loads  $N_x$  and  $N_{xy}$ , the  $30^\circ$  and  $-30^\circ$  plies are not equally loaded in their longitudinal directions; therefore, the plies do not fail contemporaneously. As indicated in the first order  $\sigma_x$ - $\tau_{xy}$  graph, the critical failure modes are the longitudinal modes in the  $-30^\circ$ ,  $30^\circ$  and  $90^\circ$  plies, respectively. Due to the interaction between the failure modes in the three plies, the second order  $\sigma_x$ - $\tau_{xy}$  curve shows a significant strength decrease compared with the first order curve. In the  $30^\circ$  and  $90^\circ$  segments, the two curves depart from each other without common tangent points. Compared with the previous test case of the  $[90^\circ/\pm 30^\circ]_S$  laminate, the current values of the uniaxial tensile and compressive strength decrease to some extent, as the unfavourable influence of a small disturbing shear load on the failure behaviour of the  $\pm 30^\circ$  pairs is taken into account.

(c) *AS4/3501-6 Quasi-isotropic Laminate*

In figure 8, the theoretical stress strain diagrams for the stress ratios  $\sigma_x:\sigma_y=1:20$  and  $\sigma_x:\sigma_y=1:2$  are plotted together with the experimental data, showing that the predictions match closely the measurements. As the shear

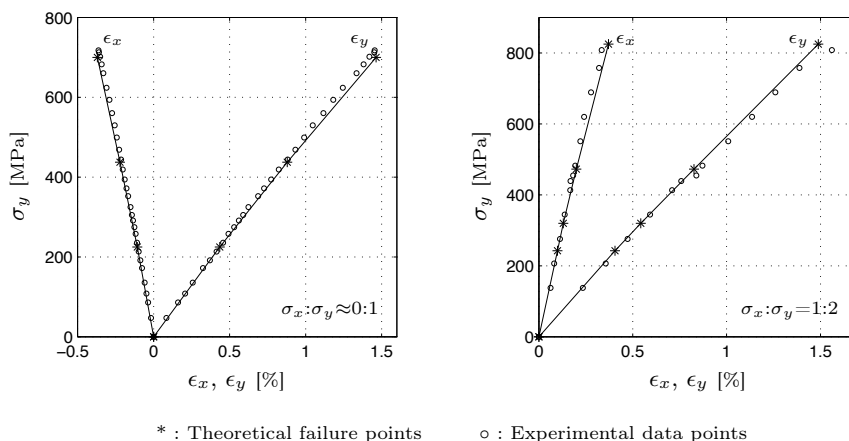


Figure 8. Stress strain diagrams of  $[0^\circ/\pm 45^\circ/90^\circ]_S$  laminate

dominated deformation mechanism that can be encountered in the  $[\pm 55^\circ]_S$  or  $[90^\circ/\pm 30^\circ]_S$  laminate plays no part in the  $[0^\circ/\pm 45^\circ/90^\circ]_S$  laminate, the reduction of the transverse modulus  $E_2$  of the  $\pm 45^\circ$  plies to 0 is superfluous. The stress strain curves are practically piecewise linear, as the non-linear effect in the shear deformations is insignificant under these loading conditions. At the failure points, the laminate stiffness decreases slightly, as the structural degradation due to the matrix cracks is almost nullified by the fibres in the perpendicular direction. In table 1, the failure stresses are summarized to enable a quantitative comparison between the theoretical and experimental results. It appears that the resolution of the experimental data points is too low to determine the initial transverse matrix failures. The good agreement between the theoretical and experimental non-catastrophic failure points implies that the residual curing stresses have limited effect on the failure behaviour of the laminate. This means that the largest part of the strain energy, which is associated with the thermal stresses, is not released during the fracture processes. In these two test cases, it can be seen that the laminate ultimate strength has been predicted with an accuracy above 97%.

In figure 9, the theoretical biaxial failure envelopes are overlaid on the experimental data for a direction comparison. For the quasi-isotropic laminate, the first order failure envelope takes a diamond shaped form, where the four sides are slightly curved because of the non-linear shear deformations in the plies. The longitudinal failure modes in the  $0^\circ$  and  $90^\circ$  plies, either tensile or compressive,

Table 1. Failure points in  $[0^\circ/\pm 45^\circ/90^\circ]_S$  laminate

| Stress ratio                    | No. | Failure mode               | Theoretical | Experimental |
|---------------------------------|-----|----------------------------|-------------|--------------|
| $\sigma_x:\sigma_y \approx 0:1$ | 1   | Transverse, $0^\circ$      | 225.0 MPa   | —            |
|                                 | 2   | Transverse, $\pm 45^\circ$ | 437.5 MPa   | 400 MPa      |
|                                 | 3   | Longitudinal, $90^\circ$   | 700.0 MPa   | 718 MPa      |
| $\sigma_x:\sigma_y = 1:2$       | 1   | Transverse, $0^\circ$      | 242.5 MPa   | —            |
|                                 | 2   | Transverse, $\pm 45^\circ$ | 320.0 MPa   | —            |
|                                 | 3   | Transverse, $90^\circ$     | 472.5 MPa   | 450 MPa      |
|                                 | 4   | Longitudinal, $90^\circ$   | 825.0 MPa   | 847 MPa      |

can be identified as the critical failure modes of the laminate. The second order failure envelope changes to an inscribed closed convex curve that is shaped as a Cartesian oval, as the longitudinal failure mode in the  $0^\circ$  plies interacts with the longitudinal failure mode in the  $90^\circ$  plies. At the tangent points of the two theoretical curves, the longitudinal stresses are equal to 0 either in the  $0^\circ$  plies or in the  $90^\circ$  plies, there is therefore no interaction between the failure modes. In spite of the large scattering in the experimental data, the predictions are found to be in good agreement with the measurements. In the compression-compression quadrant, there is evidence that the specimens failed by buckling during the tests. This explains why the theoretical curves deviate from the experimental data points in this region. In principle, the  $0^\circ$  and  $90^\circ$  plies fail simultaneously, if there holds exactly  $N_x = N_y$ . This implies that the failure mode interaction does not occur under the equal biaxial loading condition. However, one has to be conscious of the fact that these first order solutions are highly sensitive to the fluctuations in the applied loads. Generally speaking, the second order method provides better and more reliable predictions of the laminate ultimate strength.

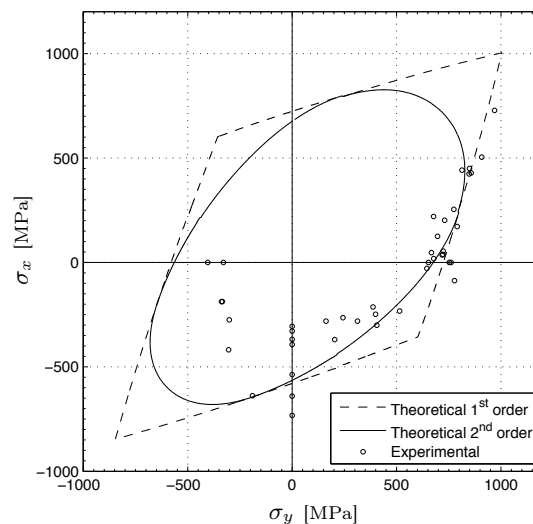


Figure 9. Failure envelope of  $[0^\circ/\pm 45^\circ/90^\circ]_S$  laminate

## 5. Conclusions and recommendations

In the present study, an attempt has been made to propose a rigorous model for the in-plane strength of laminated composites. It turns out that the lamina and laminate failure criteria can be founded on the maximum strain energy in the fundamental failure modes, where the critical failure modes are interactive and the non-critical failure modes are non-interactive. This finding enables the strength characteristics of composite laminates to be evaluated through *ab initio* calculations, where only the standard material parameters are used as input for the analysis. Through an extensive experimental verification, the progressive damage model is demonstrated to provide realistic predictions of the failure behaviour of different laminates under different loading conditions. It can be concluded that the simple model retains the essential features of the actual physical process. It should be pointed out that the generalization of the Griffith energy criterion is not intended to add an extra member to the large family of failure criteria, but to accomplish a unified criterion to supersede the established ones.

The following areas are recommended for future research:

1. For laminates under combined in-plane and out-of-plane loads, an appropriate delamination prediction algorithm has to be integrated into the progressive damage model.
2. Incorporated into a finite element program, possibly combined with an automated adaptive remeshing algorithm, the progressive damage model is expected to improve the predictability of the failure behaviour of complex composite structures.
3. In conjunction with the Monte Carlo method, the progressive damage model can be used to investigate the statistical variation in the static strength of laminates.

4. If the design strain levels of composite structures are further increased, a validated analytical fatigue life prediction methodology needs to be established; it is believed that the energy based methods remain promising for the modelling of various fatigue phenomena.
5. On a more practical level, a possible outcome of the analytical modelling efforts is the ability to develop an accurate condition monitoring system of composite structures by using a network of sensors, e.g. piezoelectric sensors.
6. Assisted by the theoretical models, various scaling techniques can be developed, enabling the failure modes of large composite structures to be simulated correctly with smaller specimens in a laboratory.
7. In a broader long-term perspective, the understanding of rapid crack propagation in composite materials and other engineering materials is clearly a grand challenge, where research at the boundaries of fracture/damage mechanics, dynamics and other related areas may lead to the unification of the two new sciences inaugurated by Galilei.

The list above is by no means complete, all interesting topics in the direction towards the mathematization of the field of mechanics of composite materials merit additional pursuit. The trend to reconcile fracture mechanics, damage mechanics, fatigue theory, buckling theory and many other related fields with each other and to subsume them within a general strength theory should be encouraged. Composite materials continue to be developed and improved to provide higher performance and there is no end in sight. In diverse industries ranging from the medical devices, sporting goods, wind energy, construction, shipbuilding to automotive and aerospace, it is beyond all doubt that human ingenuity will find more and more areas where composite materials can be beneficially utilized.

## References

- Allix O. & Hild F. (2002), *Continuum damage mechanics of materials and structures*, Elsevier, Kidlington.
- Anderson T.L. (1991), *Fracture mechanics: fundamentals and applications*, CRC Press, Boca Raton.
- Azzi V.D. & Tsai S.W. (1965), Anisotropic strength of Composites, *Exp. Mech.*, **5**, 283-288.
- Beltrami E. (1885), Sulle condizioni di resistenza dei corpi elastici, *Rend. Ist. Lomb.*, **II**, 704-714.
- Bogetti T.A., Hoppel C.P.R., Harik V.M., Newill J.F. & Burns B.P. (2004), Predicting the nonlinear response and progressive failure of composite laminates, *Compos. Sci. Technol.*, **64**, 329-342.
- Chamis C.C. (1969), Failure criteria for filamentary composites, in *Composite Materials: Testing and Design*, ASTM STP 460, American Society for Testing and Materials, Philadelphia, 336-351.
- Coulomb C.A. (1776), Essai sur une application des règles de maximis et minimis à quelques problèmes de statique, relatifs à l'architecture, *Mem. Math. Phys. Acad. Sci.*, **7**, 343-382.
- Cowin S.C. (1979), On the strength anisotropy of bone and wood, *J. Appl. Mech.*, **46**, 832-838.
- Dávila C.G., Camanho P.P. & Rose C.A. (2005), Failure criteria for FRP laminates, *J. Compos. Mater.*, **39**, 323-345.
- Dugas R. (1955), *A history of mechanics*, Éditions du Griffon, Neuchâtel, Switzerland.
- Fischer L. (1960), How to predict structural behavior of reinforced plastic laminates, *Mod. Plast.*, **37**, 121-128; 208-209.
- Galileo Galilei (1638), *Discourses on two new sciences*, Engl. Tr., Louis Elsevier, Leiden, the Netherlands.
- Griffith A.A. (1920), The phenomena of rupture and flow in solids, *Phil. Trans. R. Soc. Lond.*, **A-221**, 163-198.
- Hart-Smith L.J. (1998), Predictions of the original and truncated maximum-strain failure models, *Compos. Sci. Technol.*, **58**, 1151-1178.
- Hashin Z. (1980), Failure criteria for unidirectional fibre composites, *J. Appl. Mech.*, **47**, 329-334.
- Hencky H. (1924), Zur Theorie plastischer Deformationen und der hierdurch im Material hervorgerufenen Nachspannungen, *ZAMM*, **4**, 323-334.
- Hill R. (1948), A theory of the yielding and plastic flow of anisotropic metals, *Proc. R. Soc. Lond.*, **A-193**, 281-297.

- Hinton M.J., Kaddour A.S. & Soden P.D. (2004), *Failure criteria in fiber reinforced polymer composites: the World-Wide Failure Exercise*, Elsevier, Amsterdam.
- Hoffman O. (1967), The brittle strength of orthotropic materials, *J. Compos. Mater.*, **1**, 200-206.
- Huang K.Y., de Boer A. & Akkerman R. (2008), Analytical modeling of impact resistance and damage tolerance of laminated composite plates, *AIAA J.*, **46**, 2760–2772.
- Huang K.Y. (2019), Analytical modeling of impact resistance and damage tolerance of laminated cylindrical shells, International SAMPE Conference and Exhibition, Beijing, China.
- Huber M.T. (1904), Specific work of strain as a measure of material effort, Engl. Tr., *Tech. Trans.*, **22**, 38-81.
- Irwin G.R. (1958), Fracture, in *Handbuch der Physik*, **6**, Springer-Verlag, Berlin, 551-590.
- Jones R.M. (1998), *Mechanics of composite materials*, Taylor-Francis, Philadelphia.
- Marin J. (1957), Theories of strength for combined stresses and non-isotropic materials, *J. Aeronaut. Sci.*, **24**, 265-268.
- Meirovitch L. (1986), *Elements of vibration analysis*, McGraw-Hill, New York.
- MIL-HDBK-17 (2002), *Composite materials handbook, Polymer matrix composites: Materials usage, design, and analysis*, **3**, Department of Defense, USA.
- Miner M.A. (1945), Cumulative damage in fatigue, *J. Appl. Mech.*, **12A**, 159-164.
- von Mises R. (1913), Mechanik der festen Körper im plastisch deformablen Zustand, *Göttin Nachr Math Phys*, **3**, 582-592.
- Mohr O. (1900), Welche Umstände bedingen die Elastizitätsgrenze und den Bruch eines Materials? *ZVDI*, **24**, 1524-1530.
- Norris C.B. (1950), Strength of orthotropic materials subjected to combined stresses, Tech. Rep., U.S. Forest Products Laboratory, No. 1816.
- Orifici A.C., Herszberg I. & Thomson R.S. (2008), Review of methodologies for composite material modelling incorporating failure, *Compos. Struct.*, **86**, 194-210.
- Palmgren A. (1924), Die Lebensdauer von Kugellagern, *ZVDI*, **68**, 339-341.
- Puck A. & Schürmann H. (1998), Failure analysis of FRP laminates by means of physically based phenomenological models, *Compos. Sci. Technol.*, **58**, 1045-1068.
- Ramberg W. & Osgood W.R. (1943), Description of stress-strain curves by three parameters, Tech. Rep., National Advisory Committee for Aeronautics, Washington.
- Rankine W. (1857), On the stability of loose earth, *Phil. Trans. R. Soc. Lond.*, **147**, 9-27.

- Rowlands R.E. (1985), Strength (Failure) theories and their experimental correlation, in *Handbook of Composites, Failure Mechanics of Composites*, **3**, North-Holland, Amsterdam, 71-125.
- de Saint-Venant B. (1870), Mémoire sur l'établissement des équations différentielles des mouvements intérieurs opérés dans le corps solides ductiles au delà des limites où l'élasticité pourrait les ramener à leur premier état, *C. R. Acad. Sci.*, **70**, 473-480.
- Tresca H. (1864), Mémoire sur l'écoulement des corps solides soumis à de fortes pressions, *C. R. Acad. Sci.*, **59**, 754-758.
- Tsai S.W. & Wu E.M. (1971), A general theory of strength for anisotropic materials, *J. Compos. Mater.*, **5**, 58-80.